Mid-infrared laser-induced fluorescence with nanosecond time resolution using a superconducting nanowire single-photon detector: New technology for molecular science

Li Chen[1], Dirk Schwarzer[1], Varun B. Verma[2], Martin J. Stevens[2], Francesco Marsili[2], Richard P. Mirin[2], Sae Woo Nam[2] and Alec M. Wodtke[1]

[1] *Dept. of Dynamics at Surfaces, Max Planck Institute for Biophysical Chemistry Göttingen, Germany 37077*
[2]*National Institute of Standards and Technology, Boulder, Colorado 80305*

Email of corresponding author: awodtke@gwdg.de

Supporting information

1. Experimental setup

This section gives a more detailed description of the experimental setup. Figure S1 shows an overview perspective diagram. The sodium chloride sample crystal is mounted onto a 4-axis manipulator inside a stainless steel UHV chamber equipped with a residual gas analyser (RGA200, SRS), a leak valve, a knife blade cleaving tool and a liquid ^{4}He closed-cycle cryostat (RDK-408D2, Sumitomo), for preparation of a clean NaCl(100) single crystal surface and samples of surface adsorbed molecules. An FTIR spectrometer (Bruker 70v) is flanged to the UHV chamber to perform infrared spectroscopy of the surface adsorbates in a transmission configuration. A laser light source is directed onto the surface to excite the adsorbed sample molecules to a specific initial vibrational state (v=2), and the laser-induced infrared fluorescence photons are collected and sent through a grating monochromator and then detected by the superconducting nanowire single-photon detector (SNSPD).

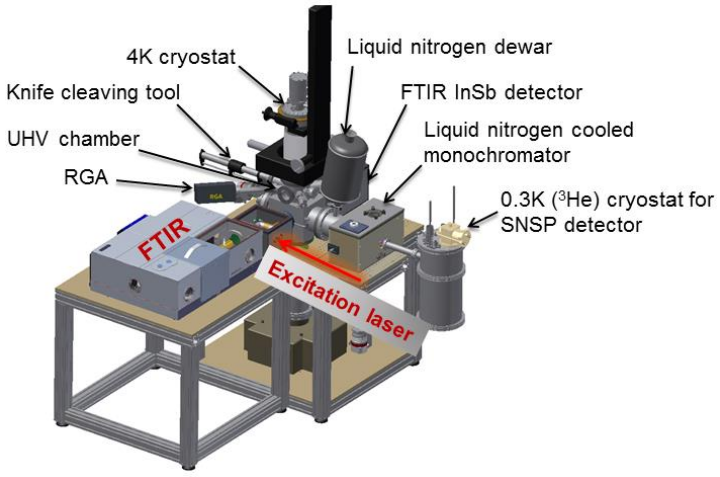

Figure S1 Experimental setup: overview.

Figure S2 illustrates the optical system for collection and detection of laser-induced infrared fluorescence signal in the mid-infrared. The fluorescence signal is first collected and collimated by an off-axis parabolic mirror (30°, effective focal length = 54.5 mm), and then focused into the entrance slit of the monochromator by another off-axis parabolic mirror (90°, effective focal length = 101.6 mm). The efficiency of the signal collection optics is limited by the numerical aperture = 0.14 of the monochromator (corresponding to an acceptance angle of 16°). At the exit of the monochromator, a multimode mid-infrared fiber is used to couple the signal to the SNSPD. The SNSPD is held at a temperature of 0.3 K in a four-stage closed-cycle cryocooler consisting of a Gifford-McMahon cryomachine (1st stage: 40 K, 2nd stage: 4 K; RDK-101D, Sumitomo) and a ^{4}He/^{3}He evaporation cooler (3rd stage: 1 K, 4th stage: 0.3 K; Chase Research Cryogenics Ltd.)

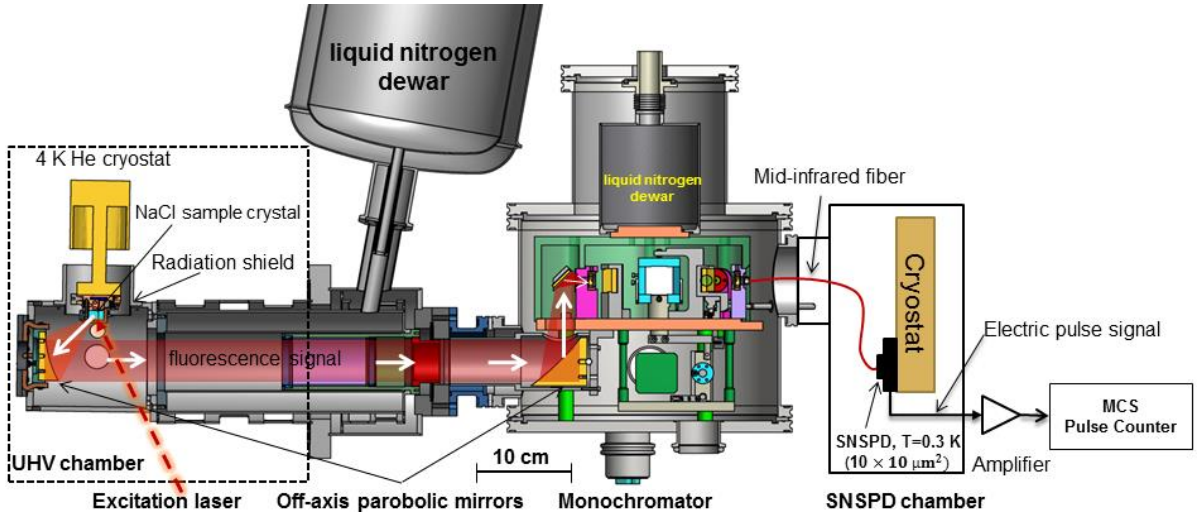

Figure S2 Experimental setup: laser-induced infrared fluorescence collection and detection.

Cooling the SNSPD to such low temperatures is essential to its optimal performance in the mid-infrared, and it is possible that the use of ^{3}He cooling is responsible for some of the reluctance to adopt this technology within the physical chemistry community. Indeed, we approached this project with a great deal of apprehension. It is important to emphasize that the initial ^{3}He charging is expensive - 2 standard liters are needed; however, even including this cost, the ^{3}He cryo-cooler is only modestly more expensive than a conventional ^{4}He cryo-cooler. Moreover, we have found this cryo-cooler to be extremely reliable over our now more than two years of experience with its operation. Most importantly, no recharging of either He reservoir has been necessary.

The excellent performance we have experienced is partly a direct result of the thermal shielding provided by the NIST cryostat design, which is shown along with parts of the ^{3}He cryocooler in Figure S3. The SNSPD is nested within a two-stage radiation shield that is integrated in a cylindrical stainless steel vacuum chamber pumped by a 70 l/s turbomolecular

pump. The outer radiation shield is bolted to the 40 K stage, the inner shield to the 4 K stage. The ^{3}He cooler is attached to the 4 K stage. The ^{3}He cooler also hangs from the 4 K plate. The SNSPD is mounted to the low temperature point of the ^{3}He cooler and is surrounded by highly reflective surfaces that are nominally at 4 K. The chalcogenide glass fiber admits the mid IR light through a vacuum feedthrough - on its way to the cryostat, the fiber is jacketed by a liquid Nitrogen cooled shield (not shown) that is thermally coupled to the monochromator assembly. The fiber itself is in thermal contact with the 40 K plate of the SNSPD's cryo-chamber.

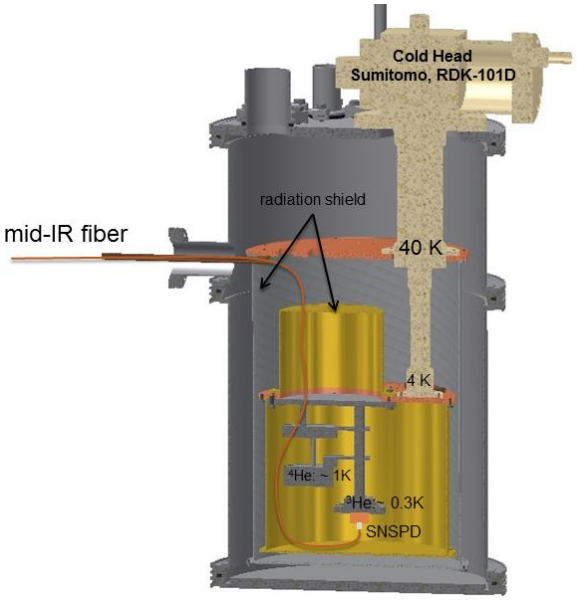

Figure S3 A cross-section view of the SNSPD cryo-chamber.

Initial cooling of the ^{4}He and ^{3}He stages from room temperature to 4.2 K takes about 15-18 hours under a vacuum better than 1 x 10^{-6} mbar. A sub-Kelvin cooling procedure is then applied to first cool the ^{4}He stage to ca. 1 K and then the ^{3}He stage (i.e., SNSPD) down to 0.25-0.3 K by evaporative cooling of liquid ^{4}He and ^{3}He. This procedure takes only about one hour, and the base temperature is held for more than 12 hours (a maximum 48 hours holding time was observed). ~~The SNSPD is itself in thermal contact with samples of evaporating liquid ^{4}He and ^{3}He that are recaptured by charcoal cryopumps.~~ Once the full charge of ^{4}He or ^{3}He has completely evaporated, the two Helium stages will warm up to 4.2 K, and the sub-Kelvin cooling procedure must be repeated in order to cool the SNSPD back to 0.3 K. Subsequently, one may continue operation for at least another 12 hours.

Sample surface cooling and heating. The sodium chloride sample crystal is mounted to an OFHC copper block attached to the cold finger of the 4 K cryostat. Two cryogenic silicon diode temperature sensors (DT-670B, Lakeshore), one mounted at the cold finger and the other at the copper block near the sample crystal, are used to monitor and control the sample

temperature. The sensor is calibrated with an accuracy better than ± 50 mK in the temperature range of 1.4 -500 K. Under UHV condition, it takes about 2.5 hours to cool down the whole sample mount from room temperature to the base temperature: 7 K at the cold finger and 11 K at the sample mount with the radiation shield at room temperature. After cooling down the radiation shield to 90 K with liquid nitrogen, the base temperatures decrease to 4 K and 6.5 K for the cold finger and the sample mount, respectively. The sample is heated via PID controlled (Model 335, Lakeshore) resistive heating of a UHV-compatible cartridge heater (50Ω, Janis Research) which is inserted into the copper block. To avoid warming up the cryostat cold finger and reduce the cooling time, the sample mount can be mechanically decoupled from the cold finger during heating and recoupled during cooling. In this way, the sample can be quickly heated up from 7 K to 400 K while the cold finger is only slightly warmed up from 4 K to 20 K, and afterwards can be cooled from 400 K to base temperature within 30 minutes.

Single NaCl (100) surface preparation and cleaning. The single NaCl (100) surface is produced by cleaving the sodium chloride sample crystal (Korth Kristalle GmbH) using the installed knife blade with a UHV base pressure level better than 1×10^{-10} mbar. After successful cleaving, the surface quality can be checked by FTIR spectroscopy of monolayer CO at the surface based on the narrow linewidth feature of the CO monolayer absorption peak. Between successive experiments, the cleanness of NaCl (100) surface can be recovered by heating the surface up to 390 K to remove any adsorbed UHV residual gas molecules (H_2, CO, CO_2 and particularly H_2O) slowly accumulated over time.

Monolayer and multilayer CO sample preparation. The monolayer and multilayer CO samples are prepared by exposing the surface to a backfilling CO pressure at controlled surface temperatures. Before the gas admission, the surface is cleaned by briefly annealing up to 390 K to remove any adsorbed UHV residual gas molecules (H_2, H_2O, CO and CO_2), and the CO gas (Sigma-Aldrich, 99% atom ^{13}C and 99% atom ^{18}O) from a lecture bottle is purified by a liquid nitrogen trap.

For monolayer CO sample preparation, the surface temperature is held at T_s= 55 K and start gas admission by slowly opening the leak valve until the UHV pressure increases to 1×10^{-6} mbar. At this temperature only the monolayer can form. Next, we turn off the surface heating while slowly closing the leak valve. We stop gas admission completely when the surface reaches T_s =35 K. This procedure for CO dosing lasts 3-5 minutes. We then hold the surface temperature at 35 K until the UHV pressure is below 5×10^{-10} mbar to prevent growth

of a CO overlayer, which starts at T_s =32 K. Afterwards, the surface is cooled further for FTIR and LIF measurements.

For multilayer CO sample preparation, the monolayer CO is first prepared and then the overlayer is grown epitaxially on top of the CO monolayer by CO dosing at T_s < 15 K. At a CO background pressure of 1 *x* 10^{-6} mbar, we observe a growth rate of 100-monolayer per minute. After the dosing, the surface is briefly annealed to 25 K for few minutes to ensure that the multilayer CO equilibrium crystal structure is formed. After the CO monolayer or multilayer sample is prepared, FTIR spectra are measured to determine the surface CO coverage as well as the frequencies of CO absorption bands for the LIF measurements afterwards.

Excitation laser system. An ~~injection-~~seeded KTP optical parametric amplifier (OPA) system is used to generate the laser light ~~source~~ for optical pumping the surface adsorbed CO molecules via the first overtone transition. The 532 nm light pulse (10 Hz, ca. 6 ns pulse width) from an injection seeded Nd: YAG laser (Continuum Surelite III) is split into two beams - one serves as the pump beam for the OPA and the other as the pump beam ~~of~~ a pulsed dye laser (Cobra - Sirah Lasertechnik GmbH). The dye (pyridine 1) laser operating at around 690 nm, together with the 532 nm pump laser, pass collinearly through two KTP crystals with the walk-off compensation arrangement in a single pass and generate a pulsed laser source tuneable in a broad wavelength range of 3900-4500 cm^{-1} (2.56-2.2 μm). With 100 mJ, 532 nm pump light and 30 mJ of the seeding dye laser light, the output signal beam pulse energy ranges from 5 mJ to 12 mJ in the whole wavelength range. The frequency of the OPA signal beam for laser excitation is calibrated by photoacoustic spectroscopy of a CO gas cell and agrees within 0.1 cm^{-1} with the rovibrational transitions of gas phase CO molecules from HITRAN database in the whole wavelength range. The laser linewidth is determined to be ca. 0.04 cm^{-1} from the measurement of the rovibrational transition linewidth.

In this experiment, the laser excitation probability is estimated to be ~3% based on the excitation laser power ca.6 mJ (4 mm in diameter) and an absorption cross section $\sigma = 5\times10^{-20}$ cm^2 $molecule^{-1}$. This absorption cross section value is estimated based on: 1) the integrated absorbance band area for overtone transition is 0.5% of the fundamental [1]; 2) the infrared absorption cross section for fundamental transition of monolayer CO on NaCl (100) [2] is $\sigma = 3\times10^{-17}$ cm^2 $molecule^{-1}$; 3) a reduction factor of 3 for multilayer absorption was introduced to account for the orientation difference of CO molecules in the monolayer and multilayer [3].

Liquid nitrogen cooled monochromator and mid-IR fiber assembly. The home-made 109 mm focal length Czerny-Turner type monochromator (Figure S4) was built into a vacuum

insulated housing suitable for liquid nitrogen cooling in order to supress blackbody radiation. At both the entrance and exit of the monochromator, liquid nitrogen cooled IR filters can be inserted to further supress background or scattered laser light. The dispersed fluorescence light is directed either to the SNSPD via the mid-IR fiber or to an InSb detector using a flip mirror operated from outside the monochromator housing by means of a vacuum feedthrough, allowing for a direct comparison of both detectors' signal levels.

The monochromator frequency is calibrated in the wavelength range of 632 nm-7594 nm (1316 cm^{-1}-15822 cm^{-1}) with an accuracy of ± 2.5 cm^{-1} using the gratings 0^{th} to 12^{th} diffraction orders of a HeNe laser single mode emission wavelength at 632.8 nm. The effective monochromator resolution is determined to be ca.12 nm with a 150 lines/mm (blazed at 4000 nm) grating and a 0.1 mm slit width.

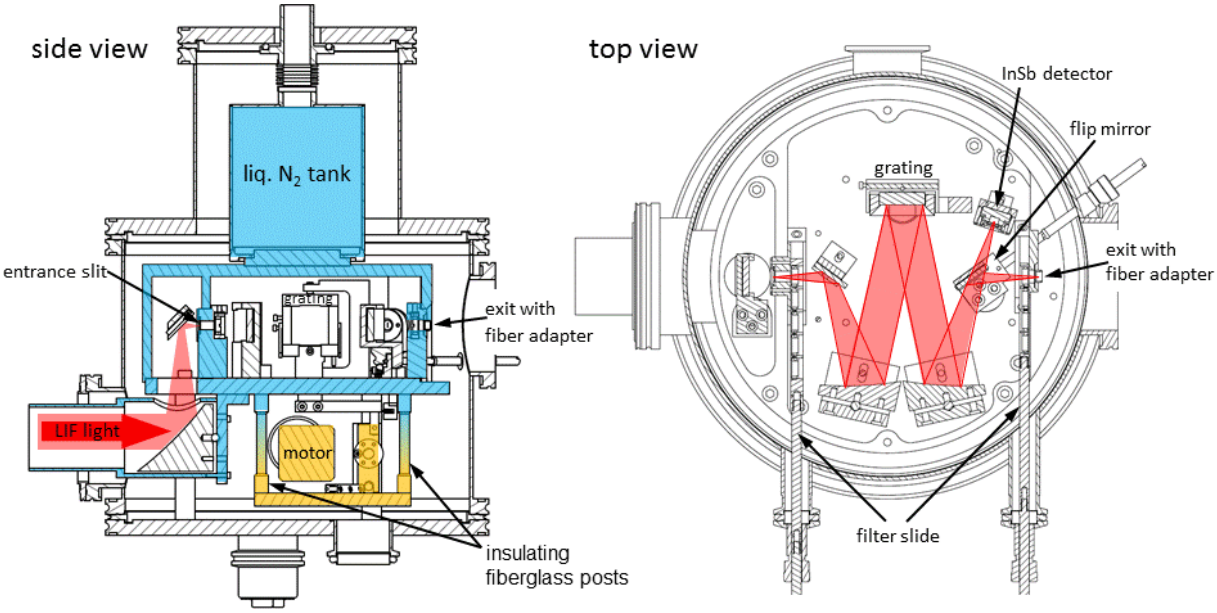

Figure S4 Cross-sectional views of the liquid nitrogen cooled monochromator

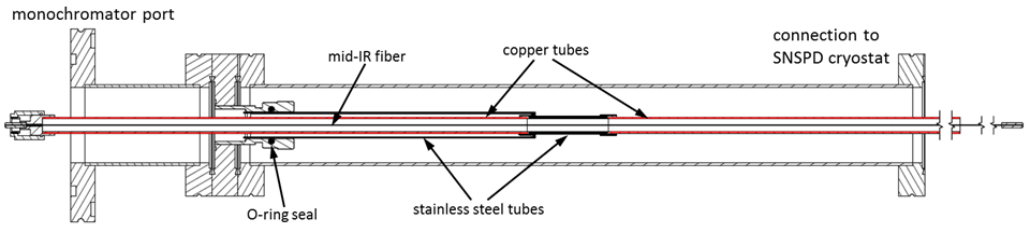

Figure S5 Mid-IR fiber assembly

Figure S5 shows the fiber assembly directing the mid-IR light from the exit of the liquid nitrogen cooled monochromator to the SNSPD. The 1 m long fiber (IRF-S-100, IRflex) ~~is~~ made of chalcogenide glass (As_2S_3), has a 100 µm diameter core and an acceptance angle of 32°. The specified internal fiber transmission is more than 99% in the 1.5-6 µm wavelength range, however, due to the high refractive index of As_2S_3 of n = 2.4, reflection losses are as

large as 31%. Moreover, due to the mismatch in size between the fiber core and the SNSPD only ~1% of the light falling on the fiber entrance reaches the SNSPD. At both ends the fiber is epoxied (Stycast 1266, Emerson & Cuming) into standard 2.5 mm zirconia ferrules. Additionally, at the monochromator side the ferrule is epoxied to an aluminium connector compatible with the FC/PC fiber adapter of the monochromator exit. To reduce blackbody radiation generated in the chalcogenide fiber due to residual absorption in the mid-IR, the whole fiber is cooled to cryogenic temperatures. This is achieved by placing the fiber, after polishing its ends, in two copper tubes interfaced by a stainless steel tube. When the fiber assembly is connected to the monochromator and the SNSPD cryostat, the copper/steel/copper tube is thermally connected on the ends to the 90 K base plate of the monochromator and the SNSPD cryostat's 40 K stage, respectively, using copper braids. To open the monochromator without breaking the vacuum of the SNSPD cryostat, a thin-walled steel tube welded to the stainless steel interface is used which fits into an O-ring sealed vacuum feedthrough (Ultra-Torr, Swagelok) of a zero-length flange closing the SNSPD cryostat.

Note that if the monochromator is held at room temperature, the SNSPD is saturated by blackbody radiation (count rate > 5 MHz) even if it is operated at a bias current as low as 4 μA. Once monochromator and external radiation shield are cooled to their base temperature (90 K) the system's background count rate is dramatically reduced. In order to determine blackbody contributions from outside and inside the monochromator, two sets of background count measurements were performed, one with the mirror in front of the monochromator exit flipped down (collecting background light from inside the monochromator) and one with the mirror up (collecting both, light from inside and outside). The left panel shows that the background count rate from inside the monochromator increases with SNSPD bias current by one order of magnitude per microamp and reaches 2 kHz at the highest bias of 6.5 μA. When the mirror is flipped up and the monochromator tuned to image 4 μm radiation from outside the monochromator to the fiber entrance, background count rate is increased by more than 1 order of magnitude. In the right panel of Figure S6 the frequency dependence of the external background count rate is plotted using a high frequency pass filter with 2150 cm^{-1} cut-off and an SNSPD bias of 6.5 μA. Background count rate peaks at 2650 cm^{-1} and drops at higher (less blackbody intensity) and lower (less SNSPD sensitivity) frequency. The external background count rate is caused by blackbody radiation from the UHV chamber scattering inside the radiation shield.

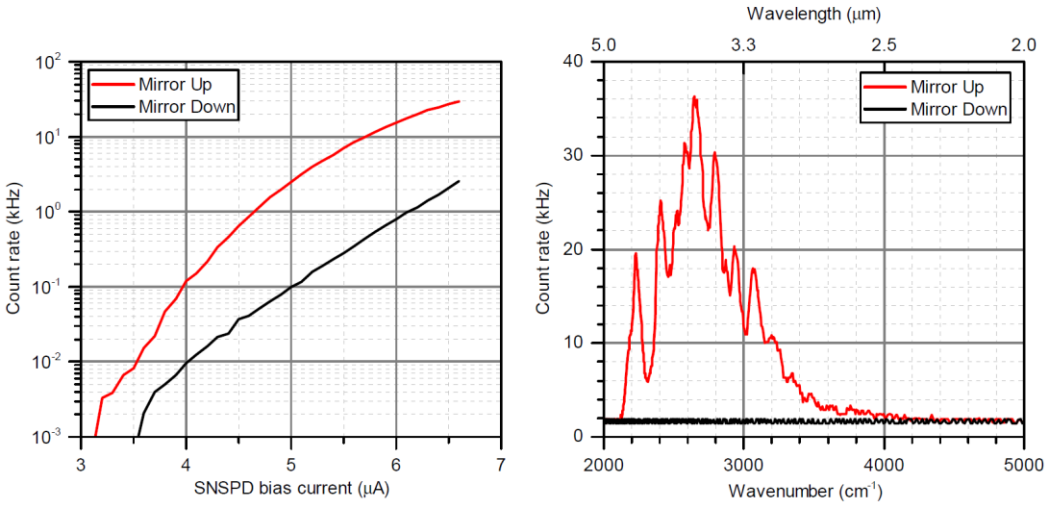

Figure S6 System background count rate with monochromator and radiation shield at base temperature (~ 90 K). Black lines: mirror in front of the monochromator exit flipped down (background from inside the monochromator); red lines: mirror up (background from inside and outside the monochromator). Left panel: background count rate vs. SNSPD bias current with monochromator fixed at 4 μm. Right panel: ~~dark~~ count rate vs. monochromator wavenumber with SNSPD bias of 6.5 μA and a 2150 cm^{-1} cut-off high frequency pass filter at the exit.

2. Mid infrared performance of the fiber-SNSPD assembly

Figure S7 shows the results of detection efficiency (DE) measurements of the fiber-SNSPD assembly used in this work. In the upper panel, we show the wavelength dependent bias current scans of the SNSPD between 2 and 6 μm. These were obtained as follows. A small fraction of the broad mid-IR output of the globar of the FTIR spectrometer (globar scattered light) is captured within the optical collection system. According to the manufacturer the globar spectrum corresponds to a 1350 K blackbody. The radiation is then monochromatized at the selected wavelength and the photon counting rate of the SNSPD is recorded as bias current is scanned from zero to the critical current. This procedure is performed with and without the presence of the globar scattered light, and the difference curve is calculated. To determine the absolute detection efficiency of the fiber-SNSPD assembly the SNSPD photon count rate is referenced to the signal produced by the InSb detector inside the monochromator (by turning the flip mirror) for which the sensitivity is specified by the manufacturer. This calibration is performed for several selected wavelengths and then transferred to other wavelength by means of the known relative globar emissivity, the wavelength-dependent monochromator transmission and the attenuation due to any IR filter used.

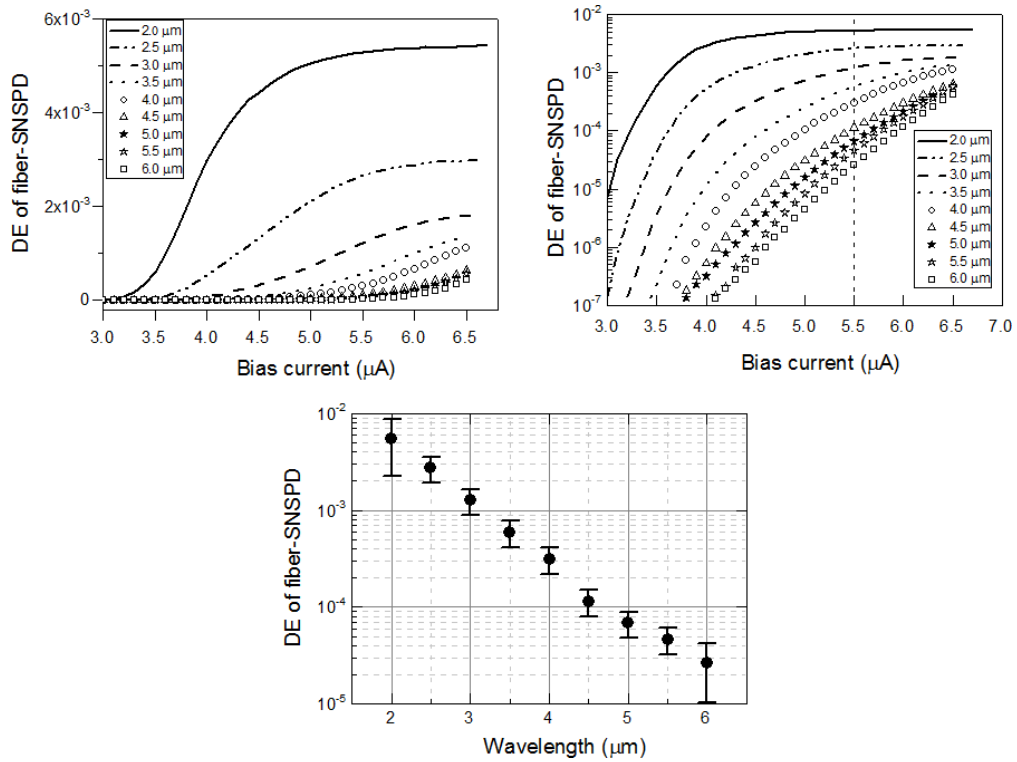

Figure S7 Wavelength and bias current dependent detection efficiency (DE) of the fiber-SNSPD assembly. Upper panels: detection efficiency vs. bias current on linear (left) and log (right) scale. Lower panel: Detection efficiency vs. wavelength at fixed bias current of 5.5 μA (relative errors are in the range 30%~~-60%~~ and result from uncertainties of the relative globar light intensity, the grating efficiency, and the InSb sensitivity.

For measurements at 2 μm, 2.5 μm and 3 μm, each curve reveals a plateau before the bias current reaches the critical current—this is generally taken as a sign that the internal efficiency of the detector is close to unity, indicating that each absorbed photon produces a counted voltage pulse. As the wavelength becomes longer, the detection efficiency decreases and the plateau feature disappears. The plateau vanishes because for longer wavelengths the deposited photon energy becomes insufficient to break superconductivity in the nanowire even at a bias close to the critical current. The drop of the detection efficiency on the plateau is caused by reduced transmission of the coupling system and absorptivity of the detector for longer wavelength.

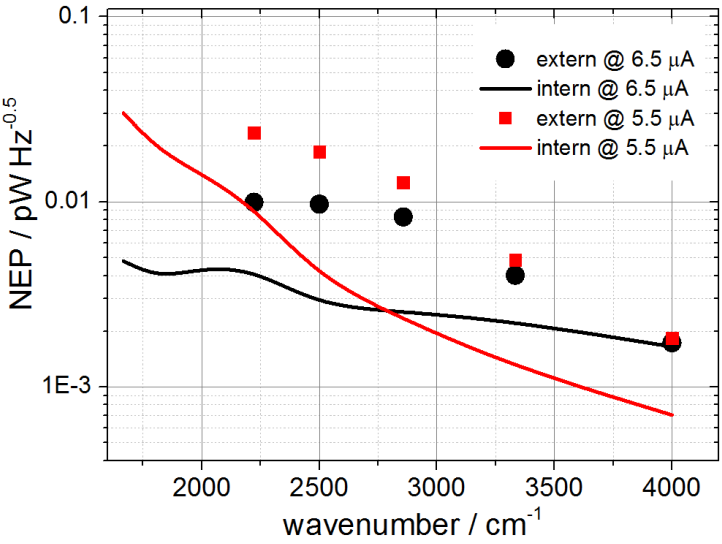

Figure S8 Noise equivalent power of the fiber-SNSPD assembly at 6.5 µA (black) and 5.5 µA (red) bias current. The calculated points include dark counts coming from outside the monochromator ~~by~~ incomplete shielding against blackbody radiation from the UHV chamber; the solid lines consider only the dark counts from inside the monochromator.

With absolute detection efficiencies *DE* (Figure S7) and background count rates R_b (Figure S6) at hand the noise equivalent power (NEP) of the fiber-SNSPD assembly is calculated[4]:

$$NEP = \frac{hc}{\lambda}\frac{1}{DE}\sqrt{2 \cdot R_b}$$

Figure S8 shows that under our present measuring conditions (black and red points) the NEP is $<2\cdot10^{-14}\ W/\sqrt{Hz}$ at 4 µm and $2\cdot10^{-15}\ W/\sqrt{Hz}$ at 2.5 µm. This may be compared with conventional nitrogen cooled InSb detectors which produce typically $10^{-12}\ W/\sqrt{Hz}$ (at dramatically reduced time resolution compared to the SNSPD). However, in contrast to the InSb detector where R_b is limited by the detector itself, in our system the noise background is dominated by blackbody radiation scattering into the radiation shield from the walls of the UHV chamber as discussed above. If we were able to improve the shielding, the NEP could be reduced. One can take the blackbody radiation emitted inside the monochromator as a lower limit to the background count rate. In that case the NEP is still background limited and would drop to $3\cdot10^{-15}\ W/\sqrt{Hz}$ at 4 µm (see lines in Figure S8). The ultimate limit would be obtained if one could get rid of the fiber (which introduces losses of 99%), place the SNSPD directly at the monochromator exit, and simultaneously suppress blackbody photons so that dark counts generated in the SNSPD itself are the only source of background counts. The enhanced detection efficiency of *DE* ~ 10% at 4 µm (bias current 6.5 µA) in combination with the SNSPD's intrinsic low noise producing dark count rates of R_b < 1 Hz[5] would lead to an NEP $\lesssim 7\cdot10^{-19}\ W/\sqrt{Hz}$.

3. Determination of relative vibrational populations

The measured dispersed fluorescence intensity temporal profiles are calibrated for the wavelength (vibrational state) dependent system detection efficiency and fluorescence rate to obtain the time evolution curves of relative vibrational population.

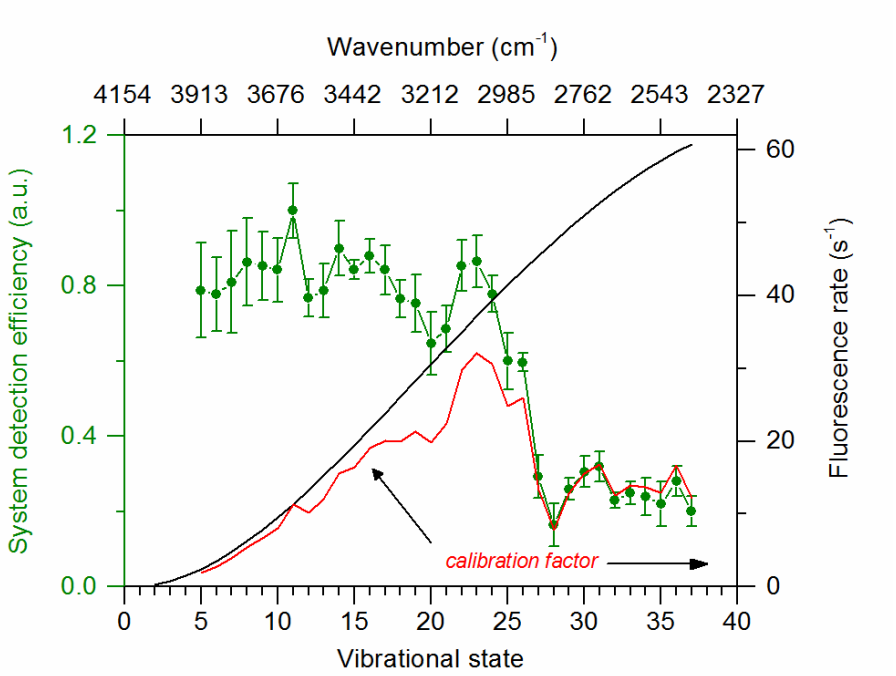

Figure S9 The vibrational state dependent system detection efficiency (green circles), fluorescence rate (black solid line) and the vibrational population calibration factor (red solid line) for $\Delta v=-2$ fluorescence signal. The error bars on the efficiency curve are from the standard deviation of five measurements.

a) Wavelength-dependent system detection efficiency

The system detection efficiency includes the monochromator grating efficiency, the fiber transmission, the IR filter transmission, the efficiency with which light is coupled into the fiber and coupled from the fiber to the SNSPD, and the SNSPD device detection efficiency. To determine the wavelength dependent system detection efficiency, a broad mid-IR light source from the globar of the FTIR spectrometer is used to mimic the laser-induced infrared fluorescence signal. Under identical experimental conditions as the fluorescence emission spectrum measurement shown in Figure 7 in the paper, the mid-IR source is used to irradiate the clean NaCl (100) surface; the scattered mid-IR light then passes through the monochromator and is detected by the SNSPD. By scanning the monochromator, a wavelength dependent intensity curve is measured. This measured intensity curve, after background subtraction (accomplished by repeated measurement with and without the globar mid-IR source), is divided by the globar's wavelength dependent intensity - this is measured by the FTIR InSb detector employing calibration of the InSb detector's wavelength dependent

sensitivity - to obtain the wavelength (or equivalently vibrational state) dependent system detection efficiency, as shown in Figure S9 (green circles).

We attribute the sudden drop of the system detection efficiency at v > 25 (below ca. 2985 cm^{-1}) to IR absorption of hydrocarbon species deposited onto the cold optics of the monochromator and the fiber ends. The hydrocarbon species may originate from the lubricant oil of the grating motor, the electric cables and thermal insulation materials inside the monchromator, for instance.

b) Fluorescence rate constants

The fluorescence rate constants (Einstein A-coefficients) for Δv=-1 ($k_n^{\Delta n=1}$), -2 ($k_n^{\Delta n=2}$) and -3 ($k_n^{\Delta n=3}$) emission states are calculated using the following equations given in Ref.[6]:

$$k_n^{\Delta n=1} = \frac{16\pi^3 \omega_{n,n-1}^3 \mu'^2}{3\varepsilon_0 hc^3} |\langle n|x|n-1\rangle|^2 \qquad (1)$$

$$k_n^{\Delta n=2} = \frac{16\pi^3 \omega_{n,n-2}^3 \mu'^2}{3\varepsilon_0 hc^3} |\langle n|x|n-2\rangle|^2 \qquad (2)$$

$$k_n^{\Delta n=3} = \frac{16\pi^3 \omega_{n,n-3}^3 \mu'^2}{3\varepsilon_0 hc^3} |\langle n|x|n-3\rangle|^2 \qquad (3)$$

where $\omega_{n,n-1}$, $\omega_{n,n-2}$ and $\omega_{n,n-3}$ are the emission frequencies for Δv = -1, -2 and -3 fluorescence, respectively. μ' is the transition dipole moment $\frac{d\mu(x)}{dx}|_{x=0}$ = 1.8 D/Å (for $^{13}C^{16}O$, see Ref.[7]). The dipole matrix elements based on Morse oscillator are given by[8]:

$$\langle n|x|n-1\rangle = \frac{1}{a(k-2n)} \left(\frac{n(k-2n-1)(k-2n+1)}{(k-n)} \right)^{1/2} \qquad (4)$$

$$\langle n|x|n-2\rangle = \frac{-1}{2a(k-2n+1)} \left(\frac{n(n-1)(k-2n-1)(k-2n+3)}{(k-n)(k-n+1)} \right)^{1/2} \qquad (5)$$

$$\langle n|x|n-3\rangle = \frac{1}{3a(k-2n+2)} \left(\frac{n(n-1)(n-2)(k-2n-1)(k-2n+5)}{(k-n)(k-n+1)(k-n+2)} \right)^{1/2} \qquad (6)$$

where a = 2.21 $Å^{-1}$ (see Ref.[7]) is the Morse potential constant and $k = \omega_e/\omega_e x_e$ is the force constant.

Based on the anharmonic constants ω_e= 2064.3 cm^{-1} and $\omega_e x_e$ = 12.12 cm^{-1} derived from the measured emission spectrum in this experiment for over-layer CO on NaCl (100), we obtain k = 170. The resulting fluorescence rate constants are plotted in Figure S10. We note

that the calculated fundamental fluorescence rate constants range from $k_1^{\Delta n=1}$ = 11.1 s^{-1} to $k_{37}^{\Delta n=1}$= 110.5 s^{-1} and the second overtone fluorescence rate constants range from $k_3^{\Delta n=3}$ = 0.007 s^{-1} to $k_{37}^{\Delta n=3}$ = 24.2 s^{-1}.

As shown in Figure S9, the calibration factors (red solid line) of vibrational states of 5 ≤ v ≤ 37 for Δv=-2 fluorescence signal are obtained by multiplying the system detection efficiency with the corresponding fluorescence rate. Then, the magnitudes of the measured dispersed fluorescence intensity temporal profiles are divided by the corresponding calibration factors to obtain the time evolution curves of relative vibrational population as shown in Figure 7 in the paper.

In addition, using the same calibration procedure, the time evolution curves of relative vibrational population for vibrational states of v=1-5 are obtained with the fluorescence intensity temporal profiles measured in Δv=-1 region. Since the kinetics of vibrational population time evolution described by Δv=-1 and Δv=-2 signal are theoretically equivalent (also checked experimentally), the two sets of vibrational population time dependent curves can be combined based on the calibration factors for v= 5→4 and v= 5→3 signals, to obtain the relative vibrational population time evolution curves for all observed vibrational states from v=1 to v=37.

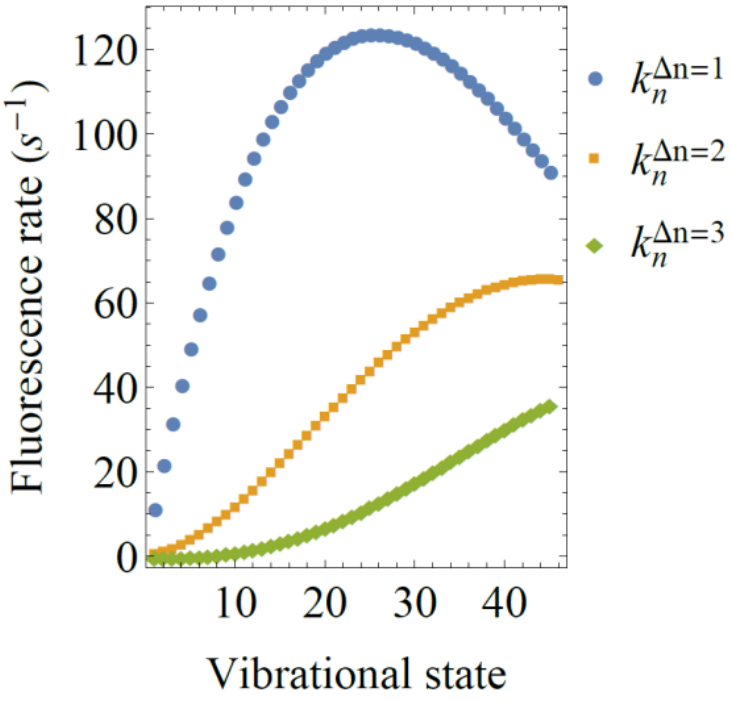

Figure S10 Fluorescence rate constants for Δv=-1 ($\boldsymbol{k_n^{\Delta n=1}}$), -2 ($\boldsymbol{k_n^{\Delta n=2}}$) and -3 ($\boldsymbol{k_n^{\Delta n=3}}$) emission.

References

(1) Dai, D. J.; Ewing, G. E. Vibrational Overtone Spectroscopy and Coupling Effects in Monolayer Co on Nacl(100). *Surf Sci* **1994**, *312*, 239-249.

(2) Chang, H. C.; Ewing, G. E. Infrared Fluorescence from a Monolayer of Co on Nacl(100). *Phys Rev Lett* **1990**, *65*, 2125-2128.

(3) Chang, H. C.; Richardson, H. H.; Ewing, G. E. Epitaxial-Growth of Co on Nacl(100) Studied by Infrared-Spectroscopy. *J Chem Phys* **1988**, *89*, 7561-7568.

(4) Korneev, A.; Matvienko, V.; Minaeva, O.; Milostnaya, I.; Rubtsova, I.; Chulkova, G.; Smirnov, K.; Voronov, V.; Gol'tsman, G.; Slysz, W.; Pearlman, A.; Verevkin, A.; Sobolewski, R. Quantum efficiency and noise equivalent power of nanostructured, NbN, single-photon detectors in the wavelength range from visible to infrared. *Ieee T Appl Supercon* **2005**, *15*, 571-574.

(5) Baek, B.; Lita, A. E.; Verma, V.; Nam, S. W. Superconducting a-WxSi1-x nanowire single-photon detector with saturated internal quantum efficiency from visible to 1850 nm. *Appl Phys Lett* **2011**, *98*, 1-3.

(6) Boney, E. T. D.; Marcus, R. A. On the infrared fluorescence of monolayer (CO)-C-13:NaCl(100). *J. Chem. Phys.* **2013**, *139*, 1-8.

(7) Corcelli, S. A.; Tully, J. C. Vibrational energy pooling in CO on NaCl(100): Methods. *J. Chem. Phys.* **2002**, *116*, 8079-8092.

(8) Gallas, J. A. C. Some Matrix-Elements for Morse Oscillators. *Phys Rev A* **1980**, *21*, 1829-1834.